Experimental and Theoretical Electron Density Study of the Peroxo Function in Oxoperoxo(pyridine-2,6-dicarboxylato)(hexamethylphosphoramide)molybdenum(VI): Implications for Olefin Epoxidation by Peroxo Transition Metal Complexes

P. Macchi,*,† A. J. Schultz,‡ F. K. Larsen,§ and B. B. Iversen*,§

Dipartimento di Chimica Strutturale e Stereochimica Inorganica, Università degli Studi di Milano, Via Venezian 21, 20133 Milano, Italy, Intense Pulsed Neutron Source, Argonne National Laboratory, Argonne, Illinois 60439, and Department of Chemistry, University of Aarhus, DK-8000 Aarhus C, Denmark

Received: April 10, 2001

The relative electrophilicity of different peroxo functions is deduced based on crystal structure correlation analysis and high-level ab initio theoretical calculations on a series of model peroxo compounds. Using electron density analysis, it is shown that peroxo functions in some organic compounds (especially dioxiranes) have a pronounced reversal of polarity resulting in a substantial electrophilic character, while in transition metal peroxides they only have an intermediate electrophilicity. The charge density of a transition metal oxidation catalyst, oxoperoxo(pyridine-2,6-dicarboxylato)(hexamethylphosphoramide)molybdenum(VI), **1**, has been determined from combined analysis of 20 K X-ray and neutron diffraction data. The good comparison with results of theoretical calculations (at the HF and B3LYP levels of theory) validates the two approaches and testifies to the suitability of experimental methods even in the presence of heavy atoms. The analysis shows that the Mo−O_{peroxo} bond contains considerable covalent character as revealed by the short Mo−O distance, the large electron density along the bond path, and the negative energy density. In **1**, the O−O distance, the atomic charges, and the electrostatic potential around the peroxo group are different from those of dioxiranes. During a direct interaction with olefins, a substantial repolarization of the group is expected to occur, possibly favored by weaker M−O bonds.

Introduction

Dioxygen complexes can be mainly categorized as either peroxo or superoxo complexes,[1] and coordination may occur as either M(η^2-O_2) or M(μ_2-O_2)M. Complexes with up to four peroxo groups coordinated to the metal are known, but the most common species are monoperoxo and diperoxo compounds.[2] The chemistry of dioxygen transition metal complexes continues to be a very active field of research, and their structure and chemical bonding have been studied in considerable detail.[2,3] Particular interest stems from the fact that many attractive applications (including industrial processes) have been found.[4] One of the most important reactions is epoxidation of olefins by peroxo complexes, and for synthetic work great sophistication has been achieved in the development of a large number of highly specific catalysts.[4] The mechanisms of olefin epoxidations are still subjects of many theoretical or experimental investigations. Two main hypotheses have dominated the discussions. The first is due to Mimoun, who suggested that the olefin coordinates to the metal center before subsequent insertion into the Mo−O bond to form a five-member metallacycle.[5] On the other hand, Sharpless suggested a concerted reaction mechanism involving a direct attack by the olefin on the peroxo oxygen atoms (with a three-member-ring intermediate).[6] In the Mimoun mechanism coordination of the olefin to the metal center (either substitution or addition) makes the olefin electrophilic[7] and thus ready for further reaction with the peroxo group acting as a nucleophile. In the Sharpless mechanism, the coordinated peroxo group is thought to have sufficiently increased its electrophilic character by decreasing the negative charge on the peroxo oxygens. A "hybrid" mechanism was proposed by Jørgensen and Hoffman, where intramolecular slipping of the olefin, after coordination to the metal, was believed to form a three-member-ring intermediate.[8]

Support for the Sharpless mechanism is often inferred from comparison with organic analogues, notably peracids and dioxiranes, which have well-accepted evidence for the electrophilic character of their peroxo function and a "Sharpless-like" mechanism in epoxidation reaction.[9,10] Rösch and co-workers have argued that η^2-coordination of O_2^{2-} species to a metal involves two opposing effects on the electrophilicity of the oxygen.[11] First, the O−O distance shortens, which makes the σ^*(O−O) orbital increase in energy and become less accessible for the olefin HOMO (π(C−C)). Second, the charge on the oxygens decreases due to charge transfer to the metal, making the peroxo group more electrophilic. The second effect is regarded as dominant, speaking in favor of a Sharpless-type mechanism, which was also supported by the calculated activation energies of different intermediates. Very recently, the strongest support of the Sharpless mechanism came from Frenking and co-workers,[12] who additionally demonstrated that a "Mimoun-like" intermediate[13] would give the carbonyl instead of the epoxide product. However, even though they may share a common mechanism in interaction with olefins (or other nucleophiles), dioxiranes, peracids, transition metal peroxo complexes, and organic peroxides are characterized by many structural and bonding differences. Therefore, we expect that their reactivity may also vary considerably. It appears timely

* Corresponding authors. E-mail: piero@csmtbo.mi.cnr.it; bo@kemi.aau.dk.
† Università degli Studi di Milano.
‡ Argonne National Laboratory.
§ University of Aarhus.

10.1021/jp011328x CCC: $20.00
Published on Web 09/19/2001

to attempt a general analysis of different oxygen−oxygen bonds in order to establish some kind of relative electrophilicity scale for the peroxo function, coupling the structural features to the electron density distribution.

A large literature exists on olefin coordination to metals, where the chemical bonding has been rationalized in terms of molecular orbital analysis and, more recently, within the framework of the quantum theory of atoms in molecules (QTAM),[14] through topological analysis of theoretical[15] and experimental[16] electron densities (ED). A similar characterization of metal−peroxo functions has not yet been carried out. The many recent papers on these complexes have examined mainly the different aspects of catalytic oxidation reactions,[11,12,17] rather than the nature of the bonding itself. One notable exception is the work by Siegbahn,[3b] who however did not use arguments based on the ED. Since theoretical models are now being widely used for describing transition metal systems, it is of general interest to constantly scrutinize the validity of the calculations. Typically they are validated by comparison with the experimentally determined crystal structures or energies of spectroscopic transitions, and more recently an increasing number of studies also compared theoretical charge distributions with experimental ground-state EDs determined from analysis of accurate X-ray diffraction data.[18] This method is by now accepted as a versatile analytical tool,[19] but only a few studies have attempted analysis of complexes with atoms beyond the first-row transition metals.[20] The major difficulties of these studies are due to the inherent loss of accuracy when dealing with compounds containing many core electrons[21] and large absorption effects, which both require high accuracy in the measurement and correction of the data. Moreover, analyses within the framework of the QTAM were not accessible due to the limitations in the current software (which cannot handle atoms with $Z > 36$). Work carried out in connection with this study[22] opens up the possibility to also routinely analyze second-row and third-row transition metal compounds. While this work was in preparation, a QTAM study of the experimental electron density in a solid containing an atom beyond first-row transition metals was published.[23]

In the present paper, we report the topological analysis of the experimental ED of $MoO(O_2)$(HMPA)(dipic) (**1**), based on a modified version[22] of the XD program.[24] The experimental ED is determined from combined analysis of conventional Ag Kα (11(1) K), synchrotron radiation (20(1) K) and time-of-flight neutron diffraction data (28(1) K); an independent X-ray experiment was also carried out at 130(2) K with Mo Kα radiation. Subsequently, the experimental ED was compared with results of high level ab initio calculations. The title compound is a typical monoperoxo complex, Figure 1, which is known to selectively catalyze the oxidation of substituted anilines to the corresponding nitrosobenzenes.[25]

The paper is structured as follows. First, we perform a structure correlation analysis of the molybdenum peroxo complexes found in crystal structure databases. We then report results from ab initio theoretical calculations on a number of model structures, comparing properties of the different peroxo functions and developing an empirical electrophilicity scale. Finally, we test the theoretical results by presenting the experimental and the theoretical ED of **1**, and discuss the implications of the results for transition metal olefin epoxidation reactions.

Experimental Section

Synthesis. Bright orange crystals of **1** were synthesized according to published procedures.[25] High-quality crystals suitable for accurate diffraction measurements were obtained by recrystallization in 2-methoxyethanol. For the neutron diffraction study large crystals were grown by seeding in saturated 2-methoxyethanol solutions of **1**. After each crystallization the largest crystals were manually cleaned for misgrowth under a microscope and the crystals showing the best extinction under polarized light were selected for further seeding. A total of more than 10 seeding cycles was necessary to obtain the final crystal specimen selected for neutron diffraction measurements (see below).

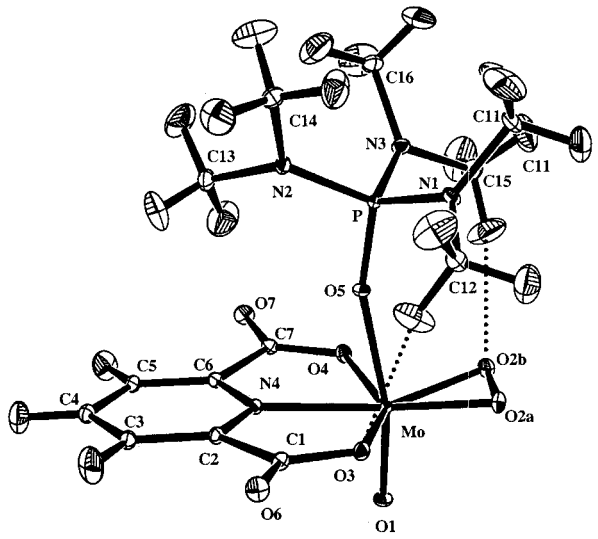

Figure 1. ORTEP view of $MoO(O_2)$(HMPA)(dipic) ($T = 20$ K). Ellipsoids are drawn at 50% level probability; the two short intramolecular C−H···O contacts (H(15a)···O(2b) = 2.311(1) Å and H(12a)···O(3) = 2.560(2) Å) are indicated as dotted lines. Note that O(2a) is involved in an intermolecular C−H···O contact (H(12c)···O(2a) = 2.583(2) Å).

20 K Synchrotron Radiation Data. A single crystal of the title compound with all dimensions smaller than 0.1 mm was mounted on a carbon fiber and placed on a Huber four-circle diffractometer at the SUNY X3A1 beam line at the National Synchrotron Light Source, Brookhaven National Laboratory. A Si(111) monochromatized beam of wavelength 0.643(1) Å was obtained from a bending magnet. The diffractometer was equipped with a Bruker CCD detector and a closed-cycle Displex helium cryostat. An antiscattering device was used to prevent parasitic scattering from the carbon composite cup, which encloses the vacuum around the target crystal.[26] Particular care was taken with cooling the sample slowly to 20(1) K in 5 h, because the crystals in some cases have been observed to break around 100 K. After cooling the rocking profiles of the diffracted intensities showed little broadening of the peaks. Due to the geometry of the goniometer, the rotation method data collection was only performed around the ϕ axis in steps of $\Delta\phi = 0.3°$ for each frame. However, the lattice symmetry (*monoclinic*) allows a good coverage of the unique reflections even with only a one-axis rotation. In addition, because of the small crystal dimensions and the relatively short wavelength used, absorption effects are small and full sphere data collection is less critical. To ensure good data redundancy, a complete (360°) ϕ oscillation was repeated several times in two different positions of the detector ($\theta = 0°$, $\theta = -58°$; 7 s per frame); the detector to sample distance was 4.670(5) cm. In each data set, the background systematically increased in two regions of ϕ, due to an unintentional slight movement of the antiscattering device from its otherwise fixed position during the ϕ oscillation. The frames acquired with this large background were discarded

together with those reflections obscured by the beam stop. The data were corrected for anisotropies (SADABS) and merged (89742 intensities, 9111 unique reflections; $R_{int} = 0.0375$; $R_\sigma = 0.0190$, $(\sin\theta/\lambda)_{max} = 0.99$ Å^{-1}). The final unit cell was determined from the positions of the intensity centroids of ca. 8000 reflections selected from the measured data: $a = 12.181(1)$, $b = 18.883(1)$, $c = 7.922(1)$ Å, $\beta = 90.48(1)°$, $V = 1822.0(5)$ Å^3.

11 K Ag Kα Radiation Data. A crystal of dimensions 0.250 × 0.175 × 0.150 mm was mounted on a Huber four-circle diffractometer equipped with a CS202 DISPLEX closed-cycle He cryostat at the Department of Chemistry, University of Aarhus. The crystal was fastened with vacuum grease inside a glass capillary and cooled in 12 h to $T = 11(1)$ K. No obvious broadening of the peaks was observed after the cooling (at variance with experiments where the crystal was fixed with glue on a glass fiber). Graphite monochromatized Ag Kα radiation ($\lambda = 0.5616$ Å) was used with the generator working at 50 kV and 40 mA. A complete hemisphere of data was collected up to $\sin\theta/\lambda = 0.60$ Å^{-1}; the strongest 1800 reflections (predicted based on a preliminary model refined on the synchrotron data) were collected up to $\sin\theta/\lambda = 1.0$ Å^{-1}. The crystal was bounded by the ±(120), ±(1−10), and ±(0−11) crystal faces; an analytical correction for absorption was applied (11 516 intensities collected, 4936 unique, $R_{int} = 0.0200$, $R_\sigma = 0.0296$). The final unit cell parameters were determined from 72 centered reflections in the range $15° < \theta < 28°$: $a = 12.180(3)$, $b = 18.874(4)$, $c = 7.932(1)$ Å, $\beta = 90.54(1)°$, $V = 1823.4(5)$ Å^3.

Merging of the Synchrotron and Tube X-ray Diffraction Data. Two preliminary models were refined based on each data set separately and used to produce intensities corrected for anomalous scattering and extinction, which are both wavelength dependent. These corrected data sets were merged into a unique data set (9882 unique data, $R_{int} = 0.0281$, $R_\sigma = 0.0303$). The final unit cell was taken as the one determined from the synchrotron data. Hereafter, we refer to the 20 K model as the one refined against these merged data.

130 K Mo Kα Radiation Data. Because of the experimental difficulties encountered in cooling the crystal below 100 K, a "reference" data collection at $T = 130(2)$ K was carried out on a 0.5 × 0.2 × 0.2 mm sample, mounted on a SMART-CCD diffractometer equipped with the Oxford N_2 gas stream low-temperature device at the Department of Chemistry, University of Aarhus. Graphite monochromatized Mo Kα ($\lambda = 0.7107$ Å) radiation was used with the generator working at 50 kV and 40 mA. No crystal breaking was observed during the cooling (60 °C/h) and during the data collection. Eight sets were collected in three different positions of the detector arm ($\theta = 0°$, $-45°$ $-60°$, with 10, 30, and 80 s per frame, respectively) using alternately ω and ϕ oscillation ($\Delta\omega$, $\Delta\phi = 0.3°$); the detector to sample distance was 3.036(1) cm. Reflections obscured by the beam stop were rejected. The final data set was corrected for absorption effects and for anisotropies (SADABS); no time decay was observed. $(\sin\theta/\lambda)_{max} = 1.04$ Å^{-1} (64 185 intensities collected, 12 632 unique, $R_{int} = 0.0252$, $R_\sigma = 0.0306$). The final unit cell was determined from the positions of ca. 8000 reflections centered after integration: $a = 12.259(1)$, $b = 18.948(4)$, $c = 7.980(1)$ Å, $\beta = 90.64(1)°$, $V = 1853.6(5)$ Å^3.

Neutron Diffraction Data. A box-shaped crystal of dimensions 1.0 × 1.2 × 4.2 mm was grown as described above and used for neutron diffraction measurements at the SCD beam line at the Intense Pulsed Neutron Source, Argonne National Laboratory. The crystal was bounded by the ±(110), ±(1−10), and ±(001) crystal faces. The measurements were carried out with the crystal wrapped tightly in aluminum foil and fastened on an aluminum pin by tiny amounts of glue, thus avoiding glue directly on the crystal. This precaution was taken based on the experience that crystals cooled for the X-ray experiments tended to crack when fastened with glue. The aluminum pin holding the sample was fitted on the cold station of a Model CS-202 DISPLEX refrigerator; which was mounted on a type 512 Huber four-circle diffractometer. The SCD beam line employs the white beam of a spallation source, and the diffractometer is equipped with a position sensitive area detector. The instrument uses ω fixed at 45°, and different volumes of reciprocal space are recorded by setting φ and χ at a number of values. A total of 29 three-dimensional data histograms (x and y spatial coordinates on the detector and the time-of-flight t) were recorded during 2 weeks of data collection restricting those reflections considered observed to those where the wavelength of the neutrons was between 0.7 and 4.2 Å. The temperature was kept fixed at 28(1) K. Local Argonne programs were used in all steps of the data acquisition, data reduction, and structure refinement.[27] The intensities were corrected for the Lorentz factor and normalized based on the measured spectral distribution of the incident beam and detector efficiency. The data were also corrected for absorption using the measured crystal morphology (μ_a(true absorption at 1.8 Å) = 1.598 cm^{-1}, μ_s-(total scattering) = 1.288 cm^{-1}). Neutron scattering lengths and absorption cross sections were taken from Sears.[28] For hydrogen, cross sections measured by Howard et al. were used.[29] Since "equivalent" reflections were recorded at different wavelengths leading to differences in, e.g., extinction, they could not be merged. The starting structural model was taken from the room-temperature X-ray study by Møller[30] with isotropic thermal parameters scaled down to approximate values at 28 K. Besides positional and thermal parameters, the refinement included separate scale factors for each of the 29 histograms. Furthermore, one isotropic extinction parameter was refined. In the final cycles a robustness criterion was used, which multiplies the minimum of (F^o/F^c, F^c/F^o) on the least-squares weights, thereby down-weighting outliers in the refinement. Further experimental details are listed in Table 1.

Multipolar Refinements. Atomic multipole expansions were assigned on each atom according to the Hansen and Coppens formalism.[31] None of the available multipolar programs could treat atoms with more than 36 electrons. Therefore, the XD code[24] was modified in order to include also 4d, 5s, and 5p orbitals both in the structure factor calculation (XDLSM, for the least-squares procedure) and in the evaluation of derived properties (XDPROP, for the topological analysis).[24] Atomic wave functions for describing core and valence orbitals were taken from Bunge et al.[32] For a second-row transition metal, the best choice should be the relativistic data set optimized from the previous wave function parameters to fit the relativistic radial scattering evaluated numerically,[33] but unfortunately data for Mo were not yet available.[34]

Mo, P, and the peroxo oxygens were expanded up to hexadecapole level; C, N, and the remaining O atoms up to octupole level; and H up to quadrupole level (with just one dipole and one quadrupole function). Positions and anisotropic thermal parameters of H were fixed at the values refined from the neutron data. A common radial scaling was applied to "chemically" equivalent atoms (one Mo, one P, five O, two C, two N; only one radial scaling type was applied for all hydrogens). For oxygen the radial scaling was not performed on the multipolar functions in accordance with a procedure suggested by Coppens and Abramov.[35] For Mo κ' and κ'' were

TABLE 1: Crystallographic Data and Refinement Residuals[a]

	host institution			
	NSLS	Univ of Aarhus	Univ of Aarhus	IPNS
radiation	X-ray	X-ray	X-ray	neutron
chemical formula	$C_{13}H_{21}MoN_4O_8P$	$C_{13}H_{21}MoN_4O_8P$	$C_{13}H_{21}MoN_4O_8P$	$C_{13}H_{21}MoN_4O_8P$
formula wt (g/mol)	488.27	488.27	488.27	488.27
T (K)	20(1)	11(1)	130(2)	28(1)
a (Å)	12.181(1)	12.180(3)	12.259(1)	12.232(3)
b (Å)	18.883(1)	18.874(4)	18.948(4)	18.941(4)
c (Å)	7.922(1)	7.932(1)	7.980(1)	7.952(1)
β (deg)	90.48(1)	90.54(1)	90.64(1)	90.55(1)
V (Å^{-3})	1822.1(5)	1823.4(5)	1853.5(5)	1842.2(5)
Z	4	4	4	4
μ_l (cm^{-1})		26.2	8.4	
T(min), T(max)		0.654, 0.711	0.751, 0.876	
λ (Å)	0.6430	0.5616	0.71073	0.74.2
space group (monoclinic)	$P2_1/n$	$P2_1/n$	$P2_1/n$	$P2_1/n$
no. reflectns collected	89 742	11 516	64 185	8 693
no. unique reflectns	9 111	4 936	12 632	8 693
R_{int}	0.0375	0.0200	0.0252	
R_σ	0.0190	0.0296	0.0306	
included in refinement ($I > 2\sigma(I)$)	9217	9217	9312	7763
no. params	784	784	784	462
R_1	0.0216	0.0216	0.0172	0.1026
R_2	0.0254	0.0254	0.0188	0.1706
wR_1	0.0248	0.0248	0.0080	
wR_2	0.0419	0.0419	0.0157	0.0671
g.o.f.	1.012	1.012	1.043	1.449

[a] $R_{int} = \Sigma|F_o^2 - F_{mean}^2|/\Sigma F_o^2$; $R_\sigma = \Sigma\sigma(F_o^2)/\Sigma F_o^2$; $R_1 = \Sigma||F_o| - |F_c||/\Sigma|F_o|$; $wR_1 = (\Sigma(F_o - F_c)^2/\Sigma wF_o^2)^{1/2}$; $R_2 = \Sigma||F_o^2| - |F_c^2||/\Sigma|F_o^2|$; $wR_2 = (\Sigma(F_o^2 - F_c^2)^2/\Sigma wF_o^4)^{1/2}$.

constrained to be equal. The radial part of the deformation density was constructed from single-ζ Slater type orbitals for C, N, O (with $n_l = 2, 2, 2, 3$), H ($n_l = 0, 1, 2$), and P ($n_l = 4, 4, 4, 6, 8$), and from HF 4d orbitals for Mo.[32] The largest residual feature of 0.3 e/Å^3 is found at the Mo nuclear position. Residual density maps are reported in the Supporting Information.

The refinement model of the 130 K data was similar except for the H atoms. Hydrogen positions were refined against the X-ray data using the method suggested by Stewart[36] and fixed in the subsequent cycles; the hydrogen deformation expansion was extended to dipolar level only and isotropic thermal parameters were refined. Further details of the multipolar refinements are listed in Table 1.

A comparison of results obtained from X-ray and neutron diffraction experiments conducted at the same temperature is often a good way to judge the quality of the data sets as well as the success of the refinement procedure (see Supporting Information). The result is, in the present case, not completely satisfactory, since the differences in thermal and positional parameters are about 3 times as large as "optimal" values reported in previous very accurate measurements.[37] Possible causes are the relatively poor quality of the neutron data (due to the presence of 21 hydrogens), the X-ray "strategy" adopted, which required a merging of two data sets[38] and the fragility of the crystal samples upon cooling below 100 K (see above). The absolute values of $\Delta\mathbf{U}$ or $\Delta\mathbf{x}$ between the X-ray and neutron experiments are relatively large for a very low temperature study, but still comparable to or smaller than typical values obtained in studies using nitrogen cooling.[37] It should also be noticed that the differences $\Delta\mathbf{U}$ or $\Delta\mathbf{x}$ are only 1.7 and 1.5 times the $\sigma(\mathbf{U})$ or $\sigma(\mathbf{x})$, since the uncertainties of parameters derived from neutron experiment are rather large. A comparison between multipolar refinements against all the X-ray data and spherical refinements of only the high order data produced better results in thermal or positional parameters.

Theoretical Calculations. Besides calculations on **1**, also some related prototype transition metal complexes, molecules, and ions were treated. The gas-phase geometry of **1** was fully optimized at the B3LYP level of theory.[39] Relativistic large-core ECPs[40] with a basis set splitting (341/321/31) and (21/21/11) were used for Mo and P, respectively; a double-ζ quality[41] and double-polarization all-electron basis (721/41/11) was used for C, N, and O; a (31) splitting was used for H (basis set I). The SCF density was computed for the molecule in the same geometry observed in the crystal; basis set I was augmented with two p functions on H and one f function on Mo[42] (basis set II). Calculations on second-row transition metal peroxides were made at B3LYP and CISD level of theory, with basis set I. For O_2, O_2^-, $(O_2)^{2-}$, HOO^-, H_2O_2, peracids, and dioxiranes, B3LYP and CISD levels with basis set II were used. The Gaussian 98 program was used in all calculations;[43] Atoms in molecules analysis was performed with PROAIM.[44] When ECPs were used, core electrons of metals were added when computing the total electron density and its properties. Frequencies were computed to check that each prototype molecule was optimized in a true minimum. However, for the optimization of **1**, frequencies could not be checked.

Structural Correlation. Crystal structure analyses were performed using the Cambridge Structural Database (CSD)[45] and the Inorganic Compounds Structural Database (ICSD).[46] The crystallographic data were screened according to the following criteria: (a) agreement index R1 < 0.100; (b) no disorder in the fragment under study; (c) no unresolved errors; (d) perfect match between chemical and crystal connectivity; (e) the presence of hydrogen bonding assigned for X−H···O contact angles larger than 120° (in intramolecular contacts, interactions between atoms separated by more than four bonds were considered).

Discussion

Structure Correlation Analysis of Molybdenum Peroxo Complexes. Molybdenum is the most abundant transition metal in published structures of peroxo complexes; 84 Mo(O_2)

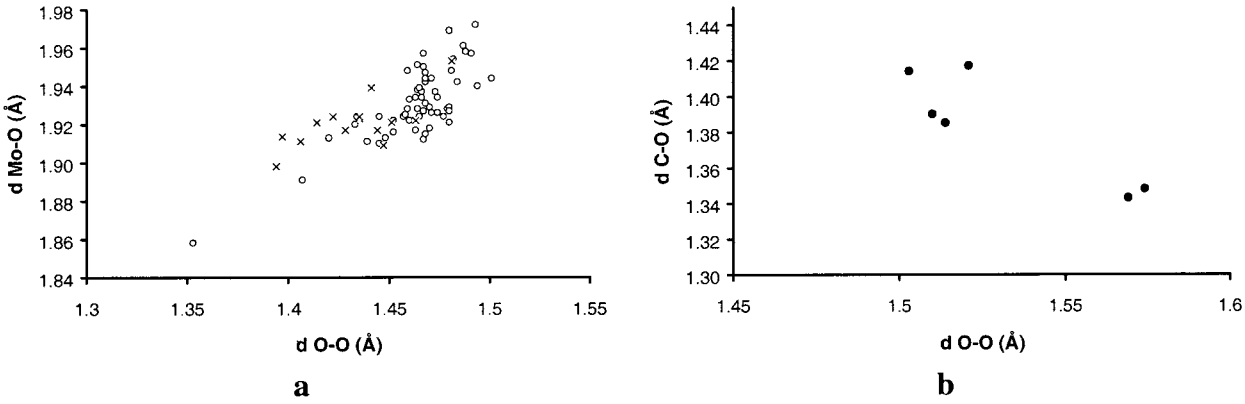

Figure 2. (a) Scatter diagram of d_{Mo-O} versus d_{O-O} for the 84 complexes retrieved from the Cambridge Structural Database (monoperoxo and diperoxo compounds are marked with crosses and circles, respectively). (b) Scatter diagram of d_{C-O} versus d_{O-O} in the few known experimentally or theoretically determined dioxiranes.[10b]

fragments (corresponding to 38 refcodes) were retrieved from the database.[45] The vast majority of the compounds are oxo−peroxo complexes, $O{=}Mo(O_2)_n$, (80 fragments, 37 refcodes). Monoperoxo coordination is found in 14 fragments (9 refcodes) with average $d_{O-O} = 1.433(7)$ Å, whereas 35 fragments (29 refcodes) are diperoxo complexes with average $d_{O-O} = 1.464(3)$ Å. The difference between mono and diperoxo complexes is also revealed in the values of IR O−O stretching frequencies, which are on average 40 cm^{-1} larger for $L_nMo(O_2)$ than for $L_mMo(O_2)_2$.[30] The longer O−O distance in diperoxo complexes correlates with their experimentally observed larger reactivity as oxidation agents.[30] In Figure 2a, Mo−O distances (d_{Mo-O}) are plotted versus O−O distances (d_{O-O}), showing a clear positive correlation between the two parameters.

The structure correlation analysis reveals other very important information. The peroxo oxygen atoms are usually involved in hydrogen bonding interactions as acceptors in X−H···O bonds (X = C, N, O). It is notable that metal peroxide complexes have shorter hydrogen bonding contacts, which occur more frequently than in organic peroxides or peracids.[47] The presence of normal hydrogen bonds in all crystal structures reveals that transition metal peroxo groups may act as nucleophiles, in striking contrast to the dioxiranes. In fact, in the crystal structure of dimesityl dioxirane, which is the only dioxirane characterized by X-ray single-crystal analysis so far,[10b] there are no hydrogen bonding interactions, the shortest intermolecular C···O contact being in excess of 3.64 Å.[48] At the same time, the O−O distance in dimesityl dioxirane is quite long (1.503(5) Å). Gas-phase microwave experiments and theoretical calculations have shown that other dioxiranes have even longer O−O distances (see Figure 2b). In addition, $Mo(O_2)$···Mo coordinations were found in eight fragments, where one of the two peroxo oxygens acts as donor (O···Mo distances are in the range 2.42−2.54 Å). This can be related to the experimental observation that transition metal peroxides may dimerize (hampering the catalytic activity).[49]

Analysis of the ED in O−O Single Bonds. To shed light on the nature of the chemical bonding in transition metal peroxo complexes, theoretical EDs on "prototype" molecules containing O−O single bonds (Scheme 1) have been investigated using the QTAM approach. Within this framework, a chemical bond is associated with a line of maximum electron density, called the *bond path* (bp), which connects two bonded atoms. The atoms are characterized as maxima of $\rho(\mathbf{r})$ and are defined in space by an atomic basin. A saddle point of $\rho(\mathbf{r})$ along the bond path is called the *bond critical point* (bcp, $\mathbf{r}_b$). Properties calculated at the bcp are often used to rationalize the nature of a chemical bond.

SCHEME 1

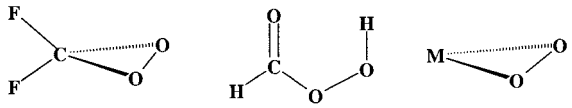

The reference O−O single bond is that in H_2O_2. According to different post-HF methods and basis sets, the optimized O−O distance is between 1.43 and 1.47 Å. This range is similar to experimental determinations in molecular crystals where H_2O_2 is either crystallized isolated or co-crystallized with other molecules (the average among experimental values is 1.459(9) Å). The O−O bcp is characterized by substantial electron density, $\rho(\mathbf{r}_b) \sim 1.8-1.9$ e $Å^{-3}$ (see Table 2), similar to the values observed in C−C single bonds. At variance with many covalent interactions, the O−O bcp has a positive value of the Laplacian ($\nabla^2\rho(\mathbf{r}_b) > 0$), thus the charge is not locally concentrated.[14] However, as first suggested by Cremer and Kraka[50] for the F_2 molecule, the total energy density $H(\mathbf{r}_b)$ is a better indicator to distinguish covalent intramolecular bonds ($H(\mathbf{r}_b) < 0$) from noncovalent intermolecular interactions ($H(\mathbf{r}_b) > 0$).[51] Single bonds between electron-rich atoms are usually elongated (due to electrostatic reasons), making the orbital overlap relatively smaller and the interaction somewhat weaker. Nevertheless, the covalency is revealed by the prevalent negative value of $H(\mathbf{r}_b)$ (see Table 2).[15]

The strong electrostatic repulsion produces a weaker interaction in the O_2^{2-} anion ($^1\Sigma_g^+$), which was shown to be metastable in the gas phase.[52] Indeed, various theoretical methods confirm the flatness of the potential energy along the O−O coordinate, though the location of the minimum is rather uncertain (d_{O-O} ranges from 1.51 to 1.65 Å, depending on the methods or the basis set adopted). Only the presence of cations can stabilize the O_2^{2-} anion in the solid state. The average d_{O-O} in ionic solids (such as Na_2O_2 and BaO_2) is 1.49(2) Å, speaking for a significant effect of the cationic field. The weakness of this O−O bond is confirmed by the topological indexes (relatively smaller $\rho(\mathbf{r}_b)$ and less negative energy density at the bcp compared to O−O in H_2O_2). Calculations on hypothetical side-on coordinated $M^{2+}(\eta^2\text{-}O_2)^{2-}$ molecules (M = Ca, Sr, etc.) gave O−O distances similar to that in the isolated O_2^{2-}. The atomic charge on the metal is close to +2 according to different partitioning schemes. After a topological analysis, two well-separated and straight M−O bond paths can be traced, as expected because the charge is mostly concentrated on the oxygens and the interaction is mainly ionic. In fact, at the bcp we find a small amount of

TABLE 2: Results of Theoretical Calculations on Some Prototype Peroxide-Containing Molecules[a]

	d_{O-O} (Å)	$\rho(\mathbf{r}_b)_{O-O}$ (e Å^{-3})	$\nabla^2\rho(\mathbf{r}_b)_{O-O}$ (e Å^{-5})	$H(\mathbf{r}_b)_{O-O}$ (h Å^{-3})	q(O)[b]	d_{X-O} (Å)	$\rho(\mathbf{r}_b)_{X-O}$ (e Å^{-3})	$\nabla^2\rho(\mathbf{r}_b)_{X-O}$ (e Å^{-5})	$H(\mathbf{r}_b)_{X-O}$ (h Å^{-3})	Δr_{X-O} (Å)
H_2O_2	1.451	1.81	5.8	−0.88	−0.47	0.968	2.49	−52.9	−4.21	−0.15
	1.437	1.87	5.4	−1.02	−0.47	0.956	2.58	−56.0	−4.49	−0.15
$(HO_AO_B)^-$	1.529	1.43	8.1	−0.55	−0.66; −0.75	0.962	2.54	−50.3	−4.13	−0.14
	1.510	1.49	8.0	−0.67	−0.65; −0.76	0.950	2.63	−53.1	−4.4	−0.14
$(O_2)^{2-}$ ($^1\Sigma_g^+$)	1.638	1.10	6.6	−0.28	−1.0					
	1.607	1.18	6.8	−0.40	−1.0					
$(O_2)^-$ ($^2\Pi$)	1.358	2.29	4.4	−1.49	−0.5					
	1.344	2.36	3.8	−1.70	−0.5					
O_2 ($^3\Sigma_g^-$)	1.213	3.51	−15.0	−4.04	0.0					
	1.202	3.60	−17.0	−4.45	0.0					
F_2CO_2	1.551	1.40	12.3	−0.55	−0.29	1.366	1.94	−12.4	−2.31	−0.18
	1.520	1.52	11.8	−0.71	−0.30	1.352	1.96	−12.4	−2.12	−0.20
$HCOO_AO_BH$	1.438	1.87	6.3	−0.93	−0.27; −0.43	1.355; 0.985	1.89; 2.35	−8.2; −50.0	−2.41; −3.98	−0.21; −0.16
	1.414	1.99	4.8	−1.15	−0.31; −0.43	1.349; 0.965	1.88; 2.48	−7.1; −56.1	−2.48; −4.45	−0.22; −0.16
$Ca(O_2)$ ($^1A_1$)	1.615	1.21	6.4	−0.42	−0.80	2.123	0.40	10.0	0.03	−0.44
	1.580	1.31	6.9	−0.53	−0.92	2.109	0.42	10.7	0.05	−0.44
$Sr(O_2)$ ($^1A_1$)	1.622	1.19	6.3	−0.41	−0.81	2.23	0.41	8.9	0.00	−0.46
	1.576	1.31	7.0	−0.53	−0.92	2.21	0.42	9.5	0.03	−0.46
$Y(O_2)$ ($^2A_1$)	1.497	1.60	8.2	−0.71	−0.63	2.005	0.79	11.0	−0.24	−0.33
	1.503	1.57	8.0	−0.76	−0.73	2.004	0.78	11.4	−0.25	−0.34
$Mo(O_2)$ ($^5B_2$)	1.447	1.83	7.8	−0.93	−0.43	1.939	0.92	12.9	−0.28	−0.22
	1.460	1.77	7.8	−0.94	−0.55	1.926	0.95	13.5	−0.32	−0.22
$Pd(O_2)$ ($^1A_1$)	1.329	2.53	2.4	−1.88	−0.28	2.030	0.68	9.8	−0.21	−0.20
	1.320	2.59	1.5	−2.08	−0.32	1.999	0.74	10.7	−0.26	−0.20

[a] For each entry, the first row refers to B3LYP/II calculations and the second to CISD/II calculations. When two values are given in a column, they are referred to the two nonequivalent oxygen atoms of the peroxide group. [b] NBO charges are reported (Mulliken charges show the very same trend; QTAM charges also have a similar trend, although with larger absolute values).

density, a positive Laplacian, and a positive energy density. Accordingly, the bcp is significantly shifted from the *nonpolar bond midpoint* toward the cation ($|\Delta\mathbf{r}_X| \sim 0.45$ Å). The nonpolar midpoint can be defined as the hypothetical midpoint of a heteroatomic bond if only covalent factors were effective.[53] A large shift of the bcp toward the cation is expected in ionic interactions. The presence of two separated bond paths is different from what occurs in prototype M···(C═C) ionic interactions (molecules such as $Cu(C_2H_4)^+$),[54] where the absence of orbital interaction results in T-shaped graphs due to the electrostatic interaction between the metal cation and the olefin π-density.

On moving to transition metals, the M−O interaction is substantially modified by the availability of d orbitals. Siegbahn[3b] calculated binding energies for oxides and peroxides of the first- and second-row transition metals. Using prototype $M(O_2)$ molecules, he demonstrated that the transfer of the peroxo oxygen can be energetically favorable, at variance with that of the oxo oxygen and in agreement with experimental evidence. Both d_{O-O} and $|q(O)|$ decrease from left to right along a row, while the M−O distance is minimal for compounds of the "central" transition metals. We have determined theoretically the electron density in the same molecules as studied by Siegbahn,[3b] and based on the topological indicators reported in Table 2, we can rationalize the following scheme (see Figure 3): (i) in early transition $M(O_2)$ compounds the bond is mainly a $(O_2)^{2-}\rightarrow M^{2+}$ donor/acceptor complex (not a pure ionic bond as in $Sr(O_2)$), (ii) "central" transition metal complexes have a larger covalent character,(iii) late transition metal complexes have more (O═O)→M complex character (largely dominated by back-donation). The larger covalency of $Mo(O)_2$ is reflected by the smaller M−O distance and $|\Delta\mathbf{r}_X|$, and by the larger $\rho(\mathbf{r}_b)$ and $|H(\mathbf{r}_b)|$. In addition, upon a NBO analysis,[55] the contribution of metal orbitals in the M−O bonds increases from Sr (less than 5%) to Mo (close to 50%). Note, however, that the larger covalency does not imply a larger binding energy, which is indeed obtained when electrostatic terms are more significant.[3b,15]

Further information can be obtained by analysis of the Laplacian distribution around the O atoms. Valence shell charge concentrations (VSCC, local maxima of the function $L(\mathbf{r}) = -\nabla^2\rho(\mathbf{r})$) can be associated with the "localization" of electron pairs (bonded or nonbonded).[14] In O_2^{2-} a "torus" of maximum $L(\mathbf{r})$ surrounds O without three-dimensional critical points due to the cylindrical symmetry of the molecule (see Figure 3). Upon coordination to the metal, the torus loses its symmetry and rank three critical points in $L(\mathbf{r})$ are created (Figure 3). In SrO_2 and YO_2, the deviations from cylindrical symmetry are very small: each O atom and its two nonbonded VSCCs lie on a plane perpendicular to the O−O bond (the VSCCs pointing opposite the metal). In MoO_2 the plane formed by the two nonbonded VSCCs and the O atom is nearly bisecting the M−O−O angle, indicating an sp^3 hybridization on O. Finally, in PdO_2 the two VSCCs are coplanar with O−O bond and opposite to O, suggesting an sp^2 hybridization. These features further confirm the bonding picture depicted above. Contrary to what was found in M[η^2-(C−C)] systems,[15,16] the molecular graph of metal−peroxo molecules is not very informative. In fact, the M−O bond paths are always slightly outwardly curved, following the oxygen orbitals responsible for the bonding. Judging from known M−O and O−O distances, "central" transition $L_nM(O_2)$ compounds conform to the more covalent model described for the prototype $Mo(O_2)$, associated with an sp^3 hybridization on the oxygens.[56] It is notable that this is the most populated class of metal peroxides in the CSD database.

For comparison other molecules containing O−O bonds were also studied (Table 2). In particular, it is important to note that in F_2CO_2 we find the largest O−O distance among compounds containing covalent O−X bonds, and these are associated with the smallest negative charge on O. Other dioxiranes show similar features, confirmed experimentally by Sander et al.,[10b] who determined the crystal structure of $(mesityl)_2CO_2$, the only dioxirane known in the CSD. Dioxiranes are highly reactive species, and many theoretical investigations have predicted an electrophilic behavior for this species.[10] According to the results

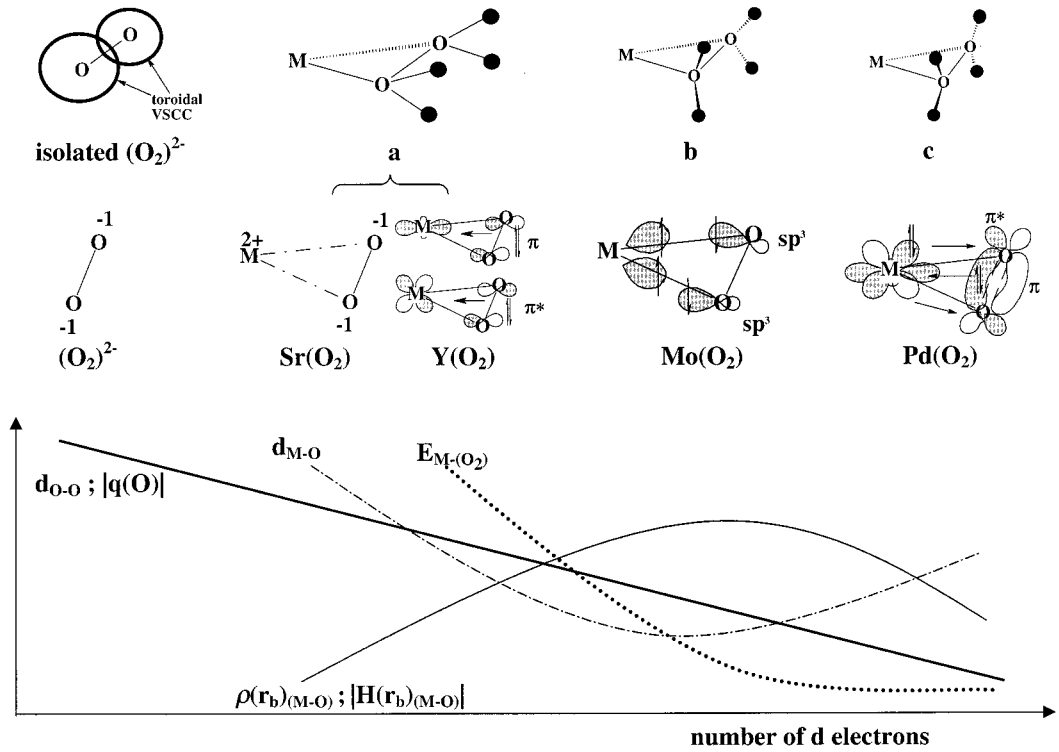

Figure 3. Overview of the topological properties of model $M(\eta^2\text{-}O_2)$ molecules. Filled circles represent the nonbonded VSCCs around peroxo oxygens; d_{O-O} and d_{M-O} are atomic distances; E_{M-O} is the bond dissocitaion energy of M−O bond (relative to neutral fragments); q(O) is the atomic charge of peroxo oxygens; $\rho(\mathbf{r}_b)_{(M-O)}$ and $H(\mathbf{r}_b)_{(M-O)}$ are the electron density and the total energy density, as evaluated at the M−O bcp.

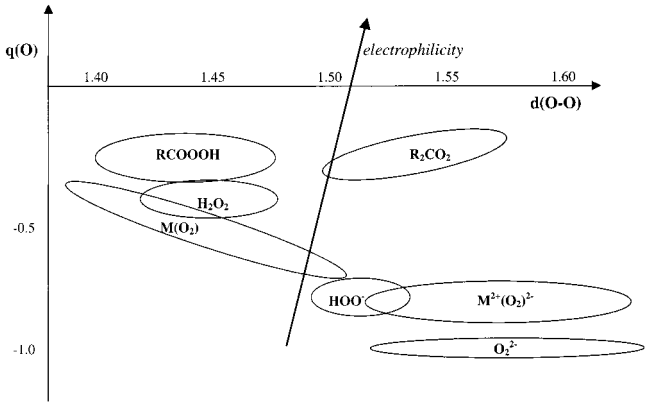

Figure 4. Qualitative electrophilicity scale of typical peroxo functions.

reported in Table 2, we can rank the O−O bond types on the basis of their electrophilic character; see Figure 4. To fit the criteria of electrophilicity, the peroxo group should have a large O−O distance, hence a low-lying σ^*(O−O) orbital (softness), and a reduced negative charge (or better a positive one) on the oxygens (hardness). According to this simple model, the peroxo function in dioxiranes is the most electrophilic, while that in $(O_2)^{2-}$ is the least. Covalent $M(O_2)$ lies in the middle of this scale and close to H_2O_2. The accumulation of negative charge in peroxo oxygens is confirmed by the electrostatic potential $\phi(\mathbf{r})$. Large negative $\phi(\mathbf{r})$ regions surround the two oxygens in $Mo(O_2)$, while only small negative regions are found around the oxygens in F_2CO_2, Figure 5a,b. Note in particular that the region of a possible nucleophilic attack (i.e., the side opposed to O−O bond) is particularly accessible in F_2CO_2. The $\phi(\mathbf{r})$ distribution in $Mo(O_2)$ is in agreement with the results of the structure correlation analysis, which show that in $L_nM(O_2)$ compounds the peroxo oxygens may act as HB acceptors (also confirmed by NMR experiments in solution[57]).

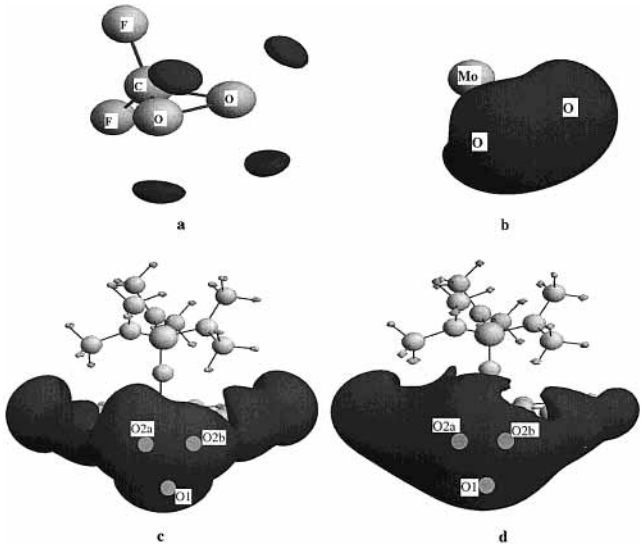

Figure 5. Electrostatic potential for (a) F_2CO_2, (b) MoO_2 calculated at CISD/II level, (c) $Mo(O_2)O$(HMPA)(dipic) calculated at the HF/II level on the experimental geometry, and (d) $Mo(O_2)O$(HMPA)(dipic) calculated from the experimental charge density. Dark isosurfaces represent negative $\phi(\mathbf{r})$ (= −0.03 e Å^{-1} in (a); = −0.1 e Å^{-1} in (b) and (c); = −0.15 e Å^{-1} in (d)); atomic nuclei are represented with light spheres (in (c) and (d) O2a, O2b, and O1 nuclei are superimposed on the electrostatic potential envelope).

Analysis of the ED in $MoO(O_2)$(HMPA)(dipic). In **1**, Mo has a pentagonal bipyramidal coordination; see Figure 1. The oxo-O1 and hexamethylphosphoramide (HMPA-O5) groups occupy the two axial sites; the pyridine-2,6-dicarboxylato (dipic) ligand is linked in three of the five equatorial positions (with O3, O4, and N4 atoms); the peroxo oxygens (O2a, O2b) bind in the two remaining equatorial sites. The Mo═O1 bond is the strongest interaction, and this has important consequences on

TABLE 3: Atomic Charges Obtained from the Monopole Coefficients (Experiment) and the HF/II Calculation on 20 K Geometry

	X-ray		
atom	20 K	130 K	HF/II
Mo	+1.37(7)	+2.10(2)	+2.82
O1	−0.75(4)	−0.63(1)	−0.65
O2	−0.61(4)	−0.49(1)	−0.49
O21	−0.60(4)	−0.43(1)	−0.52
O3	−0.54(5)	−0.53(2)	−0.65
O4	−0.64(5)	−0.50(2)	−0.63
O5	−0.84(4)	−0.51(2)	−1.11
O6	−0.12(6)	−0.26(3)	−0.42
O7	−0.12(6)	−0.28(3)	−0.42
N	−0.21(7)	−0.27(3)	−0.22
P	+0.96(9)	+0.46(6)	+2.25

the stereochemistry of the other ligands. The shortest M−O single bonds are to the peroxo oxygens, while the longest is that with the phosphoramide, which is particularly elongated due to a strong trans effect, always observed in oxo−metal compounds. In addition, the HMPA ligand is bent toward the dipic ligand, giving an experimental O═Mo−O angle of 167.6(1)° (in close agreement with the gas-phase optimized geometry). Such axial bending is found in all the fragments retrieved from CSD, with the average O═Mo−O(P) angle being 170(1)°. The oxo group also affects the equatorially bonded ligands, which are bent out of the plane perpendicular to Mo═O. In fact, the O═Mo−X angle is 102.5(1)° for the peroxo oxygens, 94.0(1)° for the carboxylic oxygens, and 90.3(1)° for the pyridinic nitrogen.[58] Among the oxo−peroxo metal compounds retrieved from the CSD, the average bending of the peroxo group is 102(1)°,[59] which is the largest value observed among all possible ligands cis to an M═O bond. The large negative regions of the electrostatic potential around these groups, which are observed experimentally[60] and theoretically, give a clear idea of the strong repulsion between atoms in the equatorial plane and O1; see Figure 5c,d. This is also supported by the distribution of atomic charges (Table 3).

The topological analysis (either on the experimental density or on the theoretical density) reveals seven separated bond paths linking Mo to the ligand atoms (Table 4). It is particularly interesting that the bond paths in the equatorial plane are all perpendicular to the Mo═O bond in the vicinity of Mo, but that they eventually "rise" when approaching the oxygens; see Figure 6. Thus the out-of-plane bending of bonds to the peroxo and carboxylato oxygens occurs at the expense of the most favorable orbitalic overlap. The Mo−O_{peroxo} and O−O bonds behave very similarly to their analogues in the Mo(O_2) prototype molecule, according to distances, $\rho(\mathbf{r}_b)$, $\nabla^2\rho(\mathbf{r}_b)$, $|H(\mathbf{r}_b)|$, and atomic charges. Among M−L single bonds, we observe that Mo−O_{peroxo} has the largest electron density and the largest $|H(\mathbf{r}_b)|$.

The electron density and the energy density evaluated at the bcp's were used in M(η^2-C_2) systems as measures for distinguishing donor−acceptor complexes from covalent metallacyclopropanes.[15] In donor−acceptor bonds $\rho(\mathbf{r}_b) \sim 0.5$ e Å^{-3} and $H(\mathbf{r}_b) \sim -0.1$ h Å^{-3}, whereas in metallacyclopropanes $\rho(\mathbf{r}_b) \sim 1.0$ e Å^{-3} and $H(\mathbf{r}_b) \sim -0.5$ h Å^{-3}. Adopting the same criterion here, we may say that the Mo−O_{peroxo} bonds are relatively more covalent, while the (C)O$^-$→Mo, (P)O→Mo and N→Mo bonds have more donor−acceptor character. However, the distinction is less pronounced, probably because the larger electronegativity difference makes the Mo−O_{peroxo} bond more polar than the M−C bonds in metallacycle systems. In the M(η^2−C_2) system, the dichotomy is between a M←(C═C) complex and a M−(C−C) metallacycle, and therefore also the shapes of the M−C bond paths are very informative. In M←(C═C) the π density is directly involved in the M−C bonding, producing an inward curvature of the bond paths, at variance from M−(C−C). In the M(η^2−O_2) system the dichotomy is between a M^{2+}←$(O_2)^{2-}$ complex and a covalent M−(O_2) metallaoxirane ring. In both cases, no O−O bonding density would be directly involved in the M−O bond, and thus the bond paths are always expected to be outwardly curved. This is in fact observed in **1**, as well as in all M(O_2) hypothetical molecules studied. On the other hand, information on the bonding situation is contained in the hybridization of the peroxo oxygens, which are expected to localize the sp^3 orbitals in a covalent metallaoxirane. As a matter of fact, on each O_{peroxo} the two nonbonded VSCCs and the O atom lie on a plane which nearly bisect the Mo−O−O angles (see Figures 3 and 7), which suggests an sp^3 hybridization (distorted due to the strained conformation adopted).

Another interesting feature is related to the disposition of Mo inner-shell charge concentrations (i-VSCC, corresponding to the Mo 4d shell), where six maxima of $L(\mathbf{r})$ are octahedrally disposed around Mo. According to the experimental orbital

TABLE 4: Properties at bcp of the Main Bonds in MoO(O_2)(hmpa)(dipic)[a]

bond X_1−X_2	$d_{X_1-X_2}$ (Å)	$\rho(\mathbf{r}_b)$ (e Å^{-3})	$\nabla^2\rho(\mathbf{r}_b)$ (e Å^{-5})	$H(\mathbf{r}_b)$ (h Å^{-3})	$\Delta\mathbf{r}_{X_1-X_2}$ (Å)
Mo−O1	1.684(1)	2.10(5)	28.2(1)	−2.10	−0.14
	1.696(1)	1.87(3)	29.88(7)	−1.59	−0.17
	1.684	1.85	19.18	−1.32	−0.18
	1.691	1.72	23.72	−1.00	−0.17
Mo−O2a	1.915(2)	0.99(4)	17.74(7)	−0.37	−0.17
	1.930(2)	0.90(2)	18.01(4)	−0.25	−0.19
	1.915	1.05	10.51	−0.42	−0.21
	1.940	0.95	11.96	−0.31	−0.21
Mo−O2b	1.914(2)	0.89(4)	16.95(8)	−0.27	−0.18
	1.929(2)	1.03(2)	17.42(3)	−0.44	−0.20
	1.914	1.05	10.62	−0.43	−0.21
	1.939	0.95	12.06	−0.31	−0.21
Mo−O3	2.053(1)	0.56(1)	12.88(1)	−0.01	−0.24
	2.062(1)	0.75(1)	12.45(1)	−0.20	−0.21
	2.053	0.72	9.43	−0.16	−0.26
	2.063	0.69	9.85	−0.13	−0.25
Mo−O4	2.043(1)	0.67(1)	12.71(1)	−0.11	−0.21
	2.053(1)	0.69(1)	12.67(1)	−0.13	−0.23
	2.043	0.74	9.60	−0.17	−0.25
	2.065	0.69	9.81	−0.13	−0.25
Mo−O5	2.130(1)	0.58(1)	10.43(1)	−0.08	−0.22
	2.140(1)	0.57(1)	9.76(1)	−0.08	−0.29
	2.130	0.52	9.35	−0.03	−0.26
	2.294	0.36	6.26	−0.03	−0.27
Mo−N4	2.136(1)	0.55(1)	9.74(1)	−0.07	−0.27
	2.138(1)	0.63(1)	8.44(1)	−0.17	−0.27
	2.136	0.67	7.07	−0.16	−0.30
	2.157	0.63	7.03	−0.13	−0.29
O2a−O2b	1.452(2)	2.03(7)	12.1(3)	−2.33	0.00
	1.460(2)	2.01(4)	9.88(14)	−2.35	0.00
	1.452	1.85	5.24	−1.06	0.00
	1.434	1.90	7.60	−1.02	0.00
P−O5	1.503(1)	2.2(1)	−15.5(8)	−3.39	−0.13
	1.506(1)	1.55(2)	−28.27(6)	−1.01	−0.28
	1.503	1.44	−29.29	−0.94	−0.29
	1.512	1.40	−29.00	−0.90	−0.29

[a] For each entry, the first line is the 20 K model, the second is the 130 K model, the third is the HF/II model on the experimental (20 K) geometry; and the fourth line is B3LYP/I model on the optimized geometry. $d_{X_1-X_2}$ is the interatomic distance; $\Delta\mathbf{r}_{X_1-X_2}$ is the shift from the nonpolar midpoint (a negative value means that the bcp is shifted toward atom X_1). Numbers in parentheses are estimated standard uncertainties. Experimental $H(\mathbf{r}_b)$ values are calculated using the empirical formula by Abramov.[68]

TABLE 5: Properties at bcp of the Remaining Bonds, Averaged over Chemically Equivalent Atoms[a]

bond X_1-X_2	$d_{X_1-X_2}$ (Å)	$\rho(\mathbf{r}_b)$ (e Å^{-3})	$\nabla^2\rho(\mathbf{r}_b)$ (e Å^{-5})	$H(\mathbf{r}_b)$ (h Å^{-3})	$\Delta\mathbf{r}_{X_1-X_2}$ (Å)
P−N	1.630(5)	1.6(1)	−10(4)	−2.0(3)	−0.23(3)
	1.635(2)	1.29(6)	−13(2)	−0.9(1)	−0.335(4)
	1.630(5)	1.272(6)	−14.6(5)	−0.98(9)	−0.347(2)
	1.660(3)	1.18(1)	−12.6(1)	−0.89(2)	−0.355(1)
$C(sp^2)-C(OO)$	1.504(1)	1.76(5)	−12(2)	−2.4(1)	0.02(6)
	1.507(1)	1.77(5)	−13.6(4)	−2.4(1)	0.01(2)
	1.504(1)	1.851(1)	−19.20(5)	−1.670(2)	0.024(1)
	1.512(1)	1.739(1)	−15.23(1)	−1.455(1)	0.019(1)
$C(sp^2)=C(sp^2)$	1.391(7)	2.20(8)	−20(1)	−3.5(2)	
	1.396(6)	2.09(3)	−17.3(6)	−3.15(8)	
	1.391(7)	2.18(4)	−25.8(9)	−2.44(9)	
	1.395(7)	2.11(4)	−22.8(9)	−2.25(9)	
$C(sp^2)-N$	1.327(3)	2.4(1)	−23(1)	−3.9(3)	−0.19(2)
	1.334(1)	2.356(3)	−26.2(3)	−3.96(8)	−0.171(2)
	1.327(3)	2.33(2)	−23.7(1)	−3.76(5)	−0.228(1)
	1.330(1)	2.298(1)	−22.84(1)	−3.39(1)	−0.207(1)
C=O	1.214(2)	2.89(7)	−13(2)	−5.0(1)	−0.21(1)
	1.218(2)	2.87(4)	−17.2(6)	−5.0(1)	−0.210(2)
	1.214(2)	2.88(1)	−12.8(5)	−5.42(3)	−0.216(0)
	1.213(1)	2.821(3)	−9.9(1)	−5.100(1)	−0.210(1)
$C-O^-$	1.313(3)	2.17(1)	−16(2)	−3.31(8)	−0.20(1)
	1.317(5)	2.23(2)	−21.8(9)	−3.6(7)	−0.179(7)
	1.313(3)	2.28(2)	−21.5(2)	−3.78(5)	−0.224(0)
	1.315(1)	2.23(1)	−19.2(1)	−3.42(1)	−0.207(1)
$C(sp^2)-H$	1.09(1)	2.0(1)	−20(4)	−3.0(4)	−0.04(3)
	1.02(3)	1.92(6)	−18(2)	−2.8(2)	−0.06(7)
	1.09(1)	1.99(4)	−29(1)	−2.3(1)	−0.034(2)
	1.088(1)	1.860(1)	−24.5(2)	−1.92(1)	0.02(1)
$C(sp^3)-N$	1.458(2)	1.74(6)	−7(1)	−2.2(1)	−0.15(3)
	1.458(5)	1.61(8)	−8(3)	−2.0(2)	−0.20(4)
	1.458(2)	1.74(1)	−17.0(2)	−1.99(4)	−0.194(8)
	1.463(5)	1.71(2)	−13.8(4)	−1.69(3)	−0.160(3)
$C(sp^3)-H$	1.088(7)	1.94(9)	−20(3)	−2.9(2)	−0.06(4)
	1.08(3)	1.7(1)	−14(2)	−2.3(3)	−0.03(6)
	1.088(7)	1.98(4)	−28(1)	−2.26(9)	−0.053(7)
	1.098(5)	1.819(3)	−22(1)	−1.81(7)	−0.011(7)

[a] Same entries as in Table 4. Numbers in parentheses are standard deviations from the average.

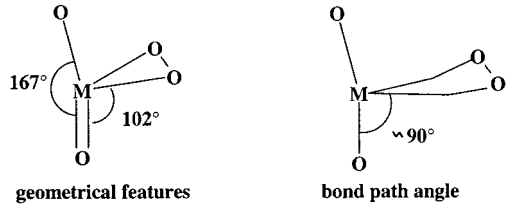

Figure 6. Comparison between internuclear vectors and bond paths in **1**.

occupancy,[61] $4d_{z^2}$ is quite populated as a consequence of the strong Mo=O bond and along the *z* direction we find two i-VSCCs (see Figure 8).[62] The slight misalignment observed seems to be a compromise to reduce the repulsion between $4d_{z^2}$ and the HMPA ligand, which would require an empty orbital, i.e., a "hole" in the Laplacian distribution, for tightening the Mo←O bond. As a result, the two i-VSCCs are "tilted" from the *z*-axis so that the i-VSCC opposed to Mo=O bond does not point directly toward O5 (the O5−Mo−i-VSCC angle is 22°); see Figure 8. In agreement with the CSD analysis, the Mo←O bond appears relatively weak. In addition, it is found that HMPA ligands trans to M=O bonds have on average M−O distances 0.07(1) Å larger than HMPA bonded cis to an oxo group. The remaining four i-VSCCs lie approximately on the equatorial plane; two of these are directed toward the peroxidic oxygens, while the other two are found between N and each O^- of the dipic ligand. This is in good agreement with the Mo−L bond types depicted above. Indeed, the most covalent

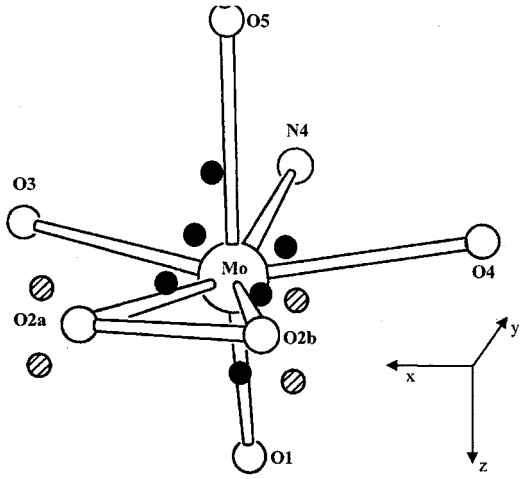

Figure 7. Disposition of i-VSCC around Mo (solid spheres) and nonbonded VSCC (shaded spheres) around peroxo oxygens in **1**. The local coordinate system used for Mo is shown.

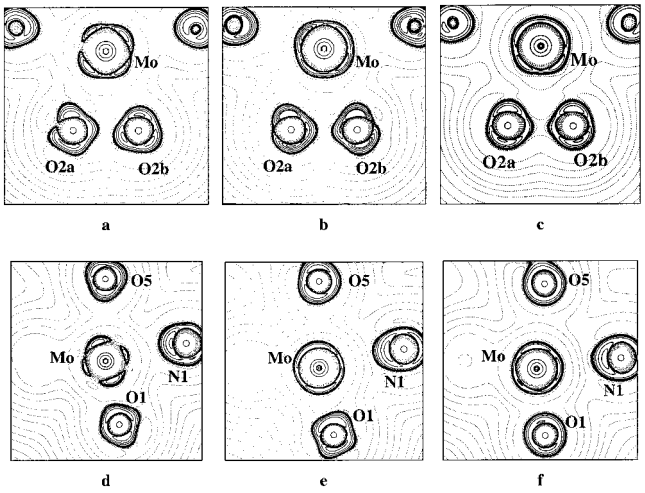

Figure 8. Laplacian distribution in Mo O2a O2b plane (a−c) and O1 Mo O5 plane (d−f). The (a) and (d) diagrams are calculated from the 20 K model, (b) and (e) are from the 130 K results and (c) and (f) are from the HF/II theoretical wave function. In each plot, contours are drawn at $\pm(1.0, 2.0, 4.0, 8.0) \times 10^x$ e Å^{-5} ($x = -2, -1, 0, 1$); solid contours represent negative Laplacian.

$Mo-O_{peroxo}$ bonds occur with i-VSCCs (produced by the more occupied d_{xy} orbital) pointing along their bond paths, while the donor−acceptor bonds occur preferentially when "holes" (produced by the least occupied $d_{x^2-y^2}$) are available for the donation. In agreement with theoretical predictions by Bader et al.,[63] the three "ligand opposed" i-VSCC (i.e., those opposed to O1, O2a, and O2b) have larger $L(\mathbf{r})$ than the "ligand directed" i-VSCC (i.e., those pointing toward O1, O2a, and O2b).

The intra- and intermolecular HBs observed in **1** (Table 6) are also worth mentioning. In agreement with crystal structure correlation analysis, O2a and O2b are involved in HBs in contrast to O1. This difference between peroxo and oxo groups supports the observation by Thiel[64] that in $L_nMO(O_2)$ compounds peroxo oxygens are more likely to be protonated than oxo oxygens. Moreover, the electrostatic potential around the peroxo oxygens is more negative than in the vicinity of the oxo group. In **1** the carboxylic oxygens also behave as HB acceptors, but all the HBs in the complex can be characterized as weak C−H···O type interactions. The two intramolecular HBs are also found in the theoretical density.

The optimized gas-phase geometry shows in general good agreement with the experimentally determined features (Tables

TABLE 6: Intra- and Intermolecular C−H···O Bonds from the Experimental 20 K Model[a]

bond	symmetry operation	$d_{C\cdots O}$ (Å)	$d_{H\cdots O}$ (Å)	C−H···O angle (deg)	$\rho(\mathbf{r}_b)$ (e Å^{-3})	$\nabla^2\rho(\mathbf{r}_b)$ (e Å^{-5})	$H(\mathbf{r}_b)$ (h Å^{-3})
H(15a)−O(2b)	(x,y,z)	3.362(1)	2.311(1)	166.0(1)	0.12(2)	1.05(5)	0.00
					0.08	1.19	0.01
H(12a)−O(3)	(x,y,z)	3.611(2)	2.560(2)	160.2(1)	0.06(2)	0.66(5)	0.01
					0.05	0.69	0.01
H(13c)−O(2b)	(x,y,z+1)	3.471(2)	2.391(1)	172.0(2)	0.03(1)	0.60(5)	0.01
H(11c)−O(6)	(−x,−y+1,−z−1)	3.433(2)	2.389(2)	161.0(2)	0.10(2)	0.78(6)	0.00
H(14a)−O(6)	(−x,−y+1,−z−1)	3.516(2)	2.538(2)	149.6(2)	0.03(1)	0.23(6)	0.00
H(12c)−O(2a)	(−x,−y+1,−z)	3.325(2)	2.583(2)	125.0(2)	0.02(1)	0.58(5)	0.01
H(14c)−O(7)	(−x+1,−y+1,−z−1)	3.499(2)	2.485(2)	154.6(2)	0.01(1)	0.31(4)	0.01
H(15b)−O(7)	(−x+1,−y+1,−z)	3.296(2)	2.588(2)	121.8(2)	0.04(1)	0.39(5)	0.01
H(3)−O(7)	(1/2+x,1/2−y,1/2+z)	3.072(2)	2.252(1)	130.2(2)	0.07(2)	0.52(5)	0.00
H(5)−O(3)	(x−1/2,1/2−y,1/2+z)	3.262(2)	2.547(2)	123.0(2)	0.03(1)	0.64(6)	0.01
H(4)−O(6)	(x−1/2,1/2−y,1/2+z)	3.514(2)	2.491(2)	154.9(2)	0.02(1)	0.42(4)	0.01

[a] For the two intramolecular bonds, the theoretical (HF/II) values are also reported (second line). Numbers in parentheses are estimated standard uncertainties.

4 and 5 as well as Supporting Information Table S2). The largest disagreement between the solid-state geometry and gas-phase optimization is found for the Mo−O(P) distance, which is 0.163 Å overestimated in the theoretical prediction (Table 4). A very similar problem was reported for a donor ligand (H_2O) opposed to the Mo═O bond (the difference was as large as 0.4 Å).[17b] It was suggested that weak donor ligands may show abrupt differences between gas phase and solid state (the weaker the donor ligand, the larger the gap). As a consequence of the overestimated distance, the Mo−O−P angle is quite different (161.4(1)° experimentally, 142.7° theoretically). The disagreement is also found in the ED along this bond. In the optimized geometry the density is nearly halved at the Mo−O5 bcp and the energy density is positive. This may suggest that in the gas phase the bond is practically a pure closed-shell electrostatic complex, while in the solid state the "compression" on this group produces also an orbital interaction.

There are qualitative differences in the descriptions of the P−O5 bond among the different models. The 20 K experimental model estimates a different contraction of the P atom, and as a consequence, the P−O and P−N bcp's are farther from P and $\rho(\mathbf{r}_b)$'s are larger than in the theoretical model or in the 130 K X-ray model (Table 5). Nevertheless, the overall agreement among the four models investigated (20 and 130 K X-ray EDs; optimized gas-phase geometry and theoretical EDs on experimental geometry) is very satisfactory and all the observations reported in the previous paragraphs appear very well founded and unbiased by the method adopted to determine the electron density. The present study definitely shows that experimental X-ray charge density analysis, including topological analysis, is possible on systems containing atoms beyond the first transition series, despite the inherent systematic errors in diffraction data of compounds containing strongly absorbing atoms with many-electron cores. Further comparative studies between theory and experiment on heavy atom structures form an important new line of research.

Implications for Olefin Epoxidation by Peroxo Transition Metal Complexes. The analysis presented above allows us to speculate about the chemical reactivity of transition metal peroxo complexes solely from knowledge of the ground-state properties. The electron density and the electrostatic potential around the peroxo function are different from those of dioxiranes. In particular, this can explain the observations that transition metal peroxides can be involved in X−H···O (X = C, N, O) bonding in the solid state (as well as in solution[57]) and in O···M coordination.

In the reactions with soft nucleophiles (such as olefins), we may expect that a repolarization of one of the two groups (C═C or O−O) is necessary. According to recent theoretical work,[11,12] the olefin coordination to the metal with subsequent attack by the peroxide (Mimoun's mechanism) was calculated to be less energetically favored and the related reaction pathway to produce a carbonyl compound instead of the epoxide. On the other hand, if the concerted three-member-ring formation is the actual intermediate (Sharpless mechanism), then it is conceivable that the repolarization must involve the whole M−(O_2) unit, since the peroxidic function alone seems to be relatively hard.

From analysis of the CSD results and the bonding scheme depicted above, we may also extract information on the factors affecting the reactivity of the different species. In a X(O−O) moiety (X = C or M) we expect that the larger the covalence in the X−O bond, the shorter the X−O distance and the less negative the charge on the oxygen (q(O)). For X = M, the strain in the M(O_2) ring is relatively small, thanks to the large bonding flexibility of transition metals (d orbitals). Thus, if the M−O bond strengthens, then the reduced negative charge on the peroxo oxygens allows a shorter O−O distance (see Figure 3) without causing larger strain in the ring. This agrees with the observed *positive* correlation between the Mo−O and O−O distances in crystal structures (Figure 2a, the correlation coefficient is +0.76(1)). M(O_2) systems are somewhat free to "move" between "a" and "b" models of the scheme in Figure 3 (i.e., from a more donor−acceptor M←$(O_2)^{2-}$ toward a more covalent metalladioxirane). This implies that d_{O-O} and q(O) change in opposite direction, and the electrophilicity of the O−O group *alone* is not substantially modified (Figure 4).[65] The increased polarizability of diperoxo complexes probably comes from the presence of weaker M−O bonds. Thus, in direct reaction with olefins, transition metal diperoxo complexes have two favorable (longer M−O and O−O bonds) and one disfavorable (larger charges on peroxo oxygens) effects compared with monoperoxo compounds.

On the other hand, in dioxiranes the sp^3 hybridization on the C atom makes the system less flexible, producing more strain in the C−O bonds. A stronger C−O bond requires a smaller strain, obtained at the expence of the O−O bond (in fact, the O−C−O angle is further enlarged, increasing d_{O-O}). Among the few known experimental or theoretical geometries of dioxirane molecules, we observe a *negative* correlation between O−O and C−O distances (see Figure 2b). Therefore, an increase in the C−O covalency directly results in a larger electrophilicity of the group because q(O) and d_{O-O} change in the same direction (Figure 4).[66] According to experimental evidence, in dioxiranes there is a tight correlation between the electrophilicity of the peroxo group and the reactivity of the molecule. Indeed,

$(mesityl)_2CO_2$ is the only compound stable enough to be crystallized; accordingly, its peroxo function has probably the smallest electrophilic character within this family of compounds.

We may conclude that the electrophilicity of the peroxo group overwhelms the C−O binding in the reactions of dioxiranes with olefins, while the strength of the M−O bond may also be a crucial parameter in reactions of metal peroxides and the repolarization occurring must therefore involve the whole $M-(O_2)$ group. Further study in this direction will be devoted to investigating details of the bonding in diperoxo complexes and the tunability of the catalysts.[67]

Concluding Remarks

In this study we have analyzed the electron density distribution in a Mo peroxide complex. Comparison of the properties derived from a theoretical model and an experimental model support the reliability of X-ray charge density even in the presence of a second transition metal atom. Prototype molecules were used to calculate bonding schemes in $M(O_2)$ moieties, and furthermore to put the observed behavior of **1** in perspective. It was shown that $M-O_{peroxo}$ bonds contain some covalent character, larger than that of the single bonds of the other ligands. Peroxo oxygens bear negative charges and are surrounded by largely negative electrostatic potential. Bonding properties and the distribution of electron density were compared to those of organic species with a peroxo function.

Although ground-state properties of the reagents cannot give the same broad insight on reaction mechanisms as full investigations of the potential energy surfaces, detailed analyses of the ED distribution can suggest the electronic and electrostatic requirements for a given mechanism to take place. We have observed that dioxiranes are more prompt to receive a nucleophilic attack from an olefin, while transition metal peroxides require a further repolarization of one of the two groups (O−O or C═C). Given the recent theoretical results,[11,12] the repolarization of the whole $M-(O_2)$ unit during the olefinic attack is the most probable, but we cannot rule out the Mimoun mechanism based only on knowledge of the ED distribution in the catalyst. On the other hand, the observations on electron density distributions in metal peroxides explains some of the nucleophilic behaviors observed for these species, such as the presence of hydrogen bond coordination in the solid state or in solution.

The present work shows that X-ray charge density analysis is a promising tool in organometallic chemistry not only for investigation of bonding types and molecular properties, but potentially also for studies of chemical reactivity. Future work will be directed toward clarifying the effects of ligand substitution and environmental (crystal) effects on the charge density of the crucial peroxo function in order to get a clearer understanding of the tunability of the catalysts.

Acknowledgment. P.M. gratefully acknowledges DANSYNC Center under the Danish Natural Science Research Council for a postdoctoral grant. The authors are indebted to Dr. G. Scalmani for his help in setting up computational software. The SUNY X3 beam line at NSLS is supported by the Division of Basic Energy Sciences of the U.S. Department of Energy (DEFG0286ER45231). Work at IPNS is supported by the U.S. Department of Energy, BES-Materials Science, under Contract No. W-31-109-ENG-38.

Supporting Information Available: Residual density plots in the Mo−O2a−O2b and Mo−O1−O5 planes, a comparison between structural parameters determined separately from the X-ray and neutron data, a table of experimental and theoretical bond distances, a summary of X−H···O contacts found in the databases, and refined multipole parameters at 20 and 130 K. This material is available free of charge via the Internet at http://pubs.acs.org.

References and Notes

(1) Vaska, L. *Acc. Chem. Res.* **1976**, *9*, 175−183.

(2) Dickman, M. H.; Pope, M. T. *Chem. Rev.* **1994**, *94*, 569−584.

(3) (a) Bytheway, I.; Hall, M. B. *Chem. Rev.* **1994**, *94*, 639−658. (b) Siegbahn, P. E. M. *J. Phys. Chem.* **1993**, *97*, 9096−9102.

(4) Jørgensen, K. A. *Chem. Rev.* **1989**, *89*, 431−458.

(5) (a) Mimoun, H.; Sereee de Roch, I.; Sajus, L. *Tetrahedron* **1970**, *26*, 37−50. (b) Mimoun, H. *Angew. Chem.* **1982**, *21*, 734−750.

(6) Sharpless, K. B.; Townsen, J. M.; Williams, D. R. *J. Am. Chem. Soc.* **1972**, *94*, 295−296.

(7) See: Eisenstein, O.; Hoffmann, R. *J. Am. Chem. Soc.* **1981**, *103*, 4308−4320 and references therein.

(8) Jørgensen, K. A.; Hoffmann, R. *Acta Chem. Scand.* **1986**, *B40*, 411−419.

(9) (a) Kwart, H.; Hoffmann, D. H. *J. Org. Chem.* **1966**, *31*, 419. (b) Plesni_ar, B.; Tasevski, M.; A_man, A *J. Am. Chem. Soc.* **1978**, 100, 743−746. (c) Freccero, M.; Gandolfi, R.; Sarzi-Amadè, M.; Rastelli, A. *J. Org. Chem.* **1999**, *64*, 3853−3860. (d) Singleton, D. A.; Merrigan, S. R.; Liu, J.; Houk, K. N. *J. Am. Chem. Soc.* **1997**, *119*, 3385−3386. (e) Yamabe, S.; Kondou, C.; Minato, T. *J. Org. Chem.* **1996**, *61*, 616−620.

(10) (a) Liu, J.; Houk, K. N.; Dinoi, A.; Fusco, C.; Curci, R. *J. Org. Chem.* **1998**, 63, 8565−8569. (b) Sander, W.; Schroeder, K.; Muthusamy, S.; Kirschfeld, A.; Kappert, W.; Boese, R.; Kraka, E.; Sosa, C.; Cremer, D. *J. Am. Chem. Soc.* **1997**, *119*, 7265−7270.

(11) (a) Di Valentin, C.; Gisdakis, P.; Yudanov, I. V.; Rösch, N. *J. Org. Chem.* **2000**, *65*, in press. (b) Gisdakis, P.; Antonczak, S.; Köstlmeier, S.; Herrmann, W. A.; Rösch, N. *Angew. Chem.* **1998**, *37*, 2211−2214. (c) Yudanov, I. V.; Gisdakis, P.; Di Valentin, C.; Rösch, N. *Eur. J. Inorg. Chem.* **1999**, 2135−2145. (d) Kühn, F. E.; Santos, A. M.; Roesky, P. W.; Herdtweck, E.; Scherer, W.; Yudanov, I. V.; Di Valentin, C.; Gisdakis, P.; Rösch, N. *Chem. Eur. J.* **1999**, *5*, 3603−3615.

(12) Deubel, D. V.; Sundermeyer, J.; Frenking, G. *J. Am. Chem. Soc.* **2000**, *122*, 10101−10108.

(13) In calculations reported in ref 12 the five-member intermediate is not formed after preliminary coordination of the olefin to the metal, but in a concerted way.

(14) Bader, R. F. W. *Atoms in molecule: A quantum theory*; Oxford University Press: Oxford, 1990.

(15) Frenking, G.; Pidum, U. *J. Chem. Soc., Dalton Trans.* **1997**, 1653−1662.

(16) Macchi, P.; Proserpio, D. M.; Sironi, A. *J. Am. Chem. Soc.* **1998**, *120*, 1447−1455 and references therein.

(17) (a) Torrent, M.; Sola, M.; Frenking, G. *Chem. Rev.* **2000**, *100*, 439−493. (b) Deubel, D. V.; Sundermeyer, J.; Frenking, G. *Inorg. Chem.* **2000**, *39*, 2314.

(18) See, for example: (a) Figgis, B. N.; Iversen, B. B.; Larsen, F. K.; Reynolds, P. A. *Acta Crystallogr., Sect. B* **1993**, *49*, 794−806. (b) Iversen, B. B.; Larsen, F. K.; Figgis, B. N.; Reynolds, P. A. *J. Chem. Soc., Dalton Trans.* **1997**, 2227−2240. (c) Schiøtt, B.; Iversen, B. B.; Madsen, G. K. H.; Bruice, T. C. *J. Am. Chem. Soc.* **1998**, *120*, 12117−12124. (d) Macchi, P.; Iversen, B. B.; Sironi, A.; Chakoumakos, B. C.; Larsen, F. K. *Angew. Chem., Int. Ed.* **2000**, *39*, 2719−2722.

(19) Coppens, P. *X-ray Charge Densities and Chemical Bonding*; Oxford Science Publications: Oxford, 1997.

(20) Figgis, B. N.; Reynolds, P. A.; Sobolev, A. N. *J. Chem. Soc., Dalton Trans.* **1994**, 1429−1433.

(21) According to (a) Coppens (Coppens, P. *Isr. J. Chem.* **1977**, *16*, 144−148) and(b), Feil (Feil, D. *Isr. J. Chem.* **1977**, *16*, 149−153), the ratio $S = V/\sum n_j^2$ (core) (V is the cell volume and n is the number of core electrons for the jth atom) is a useful measure for the suitability of ED studies (the higher the ratio is, the better the system is). First-row transition metal compounds always have very small values of S (<0.6), and for **1** $S = 0.31$. This is to be compared with values of between 1 and 6 typically observed for small organic molecules.

(22) Macchi, P. Modifications to XD code (see ref 24), unpublished.

(23) Zhurova, E. A.; Ivanov, Y.; Zavodnik, V.; Tsirelson, V. *Acta Crystallogr., Sect. B* **2000**, *B56*, 594−600. We thank an anonymous referee for bringing this reference to our attention.

(24) Koritsanszky, T.; Howard, S. T.; Su, Z.; Mallinson, P. R.; Richter, T.; Hansen, N. K. *XD, Computer Program Package for Multipole refinement and Analysis of Electron Densities from Diffraction Data*; Free University of Berlin: Berlin, Germany, June 1997.

(25) Møller, E. R.; Jørgensen, K. A. *J. Am. Chem. Soc.* **1993**, *115*, 11814−11822.
(26) Darovsky, A.; Bolotovsky, R.; Coppens, P. *J. Appl. Crystallogr.* **1994**, *27*, 1039.
(27) (a) Schultz, A. J.; Leung, P. C. W. *J. Phys (Paris) Colloq. C* **1986**, *5*, 137−142. (b) Schultz, A. J. *Trans. Am. Crystallogr. Assoc.* **1987**, *23*, 61−69.
(28) Sears, V. F. *Neutron News* **1992**, *3*, 26−37.
(29) Howard, J. A. K.; Johnson, O.; Schultz, A. J.; Stringer, A. M. *J. Appl. Crystallogr.* **1987**, *20*, 120−122.
(30) Møller, E. R. Ph.D. Thesis, Department of Chemistry, University of Aarhus, DK-8000 Århus C, Denmark, 1995.
(31) Hansen, N. K.; Coppens, P. *Acta Crystallogr., Sect. A* **1978**, *34*, 909−921.
(32) (a) Bunge, C. F.; Barrientos, J. A.; Bunge, A. V. *At. Data Nucl. Data Tab.* **1993**, *53*, 113−162. (b) Bunge, C. F.; Barrientos, J. A.; Bunge, A. V.; Cogordan, J. A. *Phys. Rev. A* **1992**, *46*, 3691−3696.
(33) Su, Z.; Coppens, P. *Acta Crystallogr.* **1998**, *A54*, 646−652.
(34) Coppens, P. State University of New York at Buffalo, personal communication.
(35) Abramov, Y.; Volkov, A.; Coppens, P. *Chem. Phys. Lett.* **1999**, *311*, 81−86.
(36) Stewart, R. F.; Bentley, J.; Goodman, B. *J. Chem. Phys.* **1975**, *63*, 3786−3793.
(37) Iversen, B. B.; Larsen, F. K.; Figgis, B. N.; Reynolds, P. A.; Schultz, A. J. *Acta Crystallogr., Sect. B* **1996**, *52*, 923−931.
(38) This strategy has previously produced better agreement with neutron data. See, for example: Overgaard, J.; Schiøtt, B.; Larsen, F. K.; Schultz, A. J.; MacDonald, J. C.; Iversen, B. B. *Angew. Chem., Int. Ed. Engl.* **1999**, *38*, 1239−1242.
(39) Becke, A. D. *J. Chem. Phys.* **1993**, *98*, 5648.
(40) Hay, P. J.; Wadt, W. R. *J. Chem. Phys.* **1985**, *82*, 299.
(41) Dunning, T. H.; Hay, P. J. *Modern Theoretical Chemistry*; Schaefer, H. F. III, Ed.; Plenum: New York, 1976; Vol. 3, p 1.
(42) ζ was taken from: Ehelers, A. W.; Böhme, M.; Dapprich, S.; Gobbi, A.; Höllwarth, A.; Jonas, V.; Köhler, K. F.; Stegmann, R.; Veldkamp, A.; Frenking, G. *Chem. Phys. Lett.* **1993**, *208*, 111−114.
(43) Frisch, M. J.; Trucks, G. W.; Schlegel, H. B.; Scuseria, G. E.; Robb, M. A.; Cheeseman, J. R.; Zakrzewski, V. G.; Montgomery, J. A.; Stratmann, R. E.; Burant, J. C.; Dapprich, S.; Millam, J. M.; Daniels, A. D.; Kudin, K. N.; Strain, M. C.; Farkas, O.; Tomasi, J.; Barone, V.; Cossi, M.; Cammi, R.; Mennucci, B.; Pomelli, C.; Adamo, C.; Clifford, S.; Ochterski, J.; Petersson, G. A.; Ayala, P. Y.; Cui, Q.; Morokuma, K.; Malick, D. K.; Rabuck, A. D.; Raghavachari, K.; Foresman, J. B.; Cioslowski, J.; Ortiz, J. V.; Baboul, A. G.; Stefanov, B. B.; Liu, G.; Liashenko, A.; Piskorz, P.; Komaromi, I.; Gomperts, R.; Martin, R. L.; Fox, D. J.; Keith, T.; Al-Laham, M. A.; Peng, C. Y.; Nanayakkara, A.; Gonzalez, C.; Challacombe, M.; Gill, P. M. W.; Johnson, B.; Chen, W.; Wong, M. W.; Andres, J. L.; Gonzalez, C.; Head-Gordon, M.; Replogle, E. S.; Pople, J. A. *Gaussian 98*; Gaussian, Inc.: Pittsburgh, PA, 1998.
(44) Biegler-König, F. W.; Bader, R. F. W.; Ting-Hua, T. *J. Comput. Chem.* **1982**, *3*, 317.
(45) Cambridge Crystallographic Data Centre, June 2000.
(46) Berndt, M. ICSD/RETRIEVE 1990−1997.
(47) The statistical occurrence (frequency) of X−H···O contacts (X = C, N, O) in $L_mMo(O_2)_n$ complexes is more than twice as large as in organic peroxides (ROOR). In addition, both the shortest and the average X···O distances are smaller (see Supporting Information).
(48) In metal peroxides, C−H···O contacts have an average $d_{C\cdots O}$ = 3.32(8) Å, with the shortest contacts being 3.15 Å (see Supporting Information).
(49) Wahl, G.; Kleinhenz, D.; Schorm, A.; Sundermeyer, J.; Stowasser, R.; Rummey, C.; Bringmann, G.; Fickert, C.; Kiefer, W. *Chem. Eur. J.* **1999**, *5*, 3237−3251.
(50) (a) Cremer, D.; Kraka, E. *Croat. Chem. Acta* **1984**, *57*, 1259−1281. (b) Cremer, D.; Kraka, E. *Angew. Chem., Int. Engl. Ed.* **1984**, *23*, 67−68.
(51) $H(\mathbf{r}) = G(\mathbf{r}) + V(\mathbf{r})$, where $G(\mathbf{r})$ and $V(\mathbf{r})$ are the kinetic and the potential energy density, respectively. Since everywhere $G(\mathbf{r}) > 0$ and $V(\mathbf{r}) < 0$, a negative $H(\mathbf{r})$ indicates a dominant contribution of $V(\mathbf{r})$, and this was put in relation to the covalency of a bond (see refs 14and 50).
(52) Nakatsuji, H.; Nakai, H. *Chem. Phys. Lett.* **1992**, *197*, 339−345. Note that O_2^{2-} is not known in the gas phase.
(53) In a A_1–A_2 bond, the distance of the nonpolar midpoint from atom A_1 is $m_{A_1} = r_1 r_{12}(r_1 + r_2)^{-1}$ where r_1 and r_2 are the covalent radii of atoms A_1 and A_2, respectively, r_{12} is the A_1–A_2 distance; $\Delta r_{A_1} = d_1 - m_1$ is the shift of the bcp from the nonpolar midpoint, where d_1 is the distance of the bcp from atom A_1. See: Otto, M.; Lotz, S. D.; Frenking, G. *Inorg. Chem.* **1992**, *31*, 3647−3655.
(54) Böhme, M.; Wagener, T.; Frenking, G. *J. Organomet. Chem.* **1996**, *520*, 31−43.
(55) Carpenter, J. E.; Weinhold, F. *J. Mol. Struct. (THEOCHEM)* **1988**, *169*, 41.
(56) However, the few early and late transition metal $L_nM(O_2)$ examples retrieved from the database do not show the extreme behavior computed for their $M(O_2)$ prototypes, but are rather similar to $Mo(O_2)$. It is notable that no group 3 or group 10 peroxide is known in the CSD; only four group 4 and eight group 9 compounds have been reported.
(57) Glas, H.; Spiegler, M.; Thiel, W. R. *Eur. J. Inorg. Chem.* **1998**, 275−281.
(58) In the gas-phase optimized geometry, these angles are 104.6°, 95.0°, and 92.2, respectively.
(59) In the CSD there are a few exceptions with O═M−O < 90°, but these were found to be errors in the database entries, occurring when ═O and H_2O ligands are trans to each other and the chemical types of the O atoms have been erroneously interchanged.
(60) Calculated according to: Su, Z.; Coppens, P. *Acta Crystallogr., Sect. A* **1992**, *A48*, 188.
(61) At 20 K the d-orbital populations derived from the multipole coefficients according to Holladay et al. (Holladay, A.; Leung, P.; Coppens, P. *Acta Crystallogr., Sect. A* **1983**, *A39*, 377−387) are d_{z^2} = 1.53(2), d_{xz} = 1.00(2), d_{yz} = 0.64(2), $d_{x^2-y^2}$ = 0.38(2), d_{xy} = 1.08(3).
(62) The *z* axis is directed along the M═O bond. *x* and *y* are approximately directed toward N4 and O3, respectively; see Figure 7.
(63) Bader, R. F. W.; Gillespie, R. J.; Martin, F. *Chem. Phys. Lett.* **1998**, *290*, 488−494.
(64) Thiel, W. R. *J. Mol. Catal. A* **1997**, *117*, 449−454.
(65) This is confirmed by preliminar theoretical calculations (at HF/II level) on the prototype diperoxo compound, namely, the "Mimoun complex" $MoO(O_2)_2(HMPA)(H_2O)$, using the experimental crystal geometry. (a) Le Carpentier, J.-M.; Schlupp, R.; Weiss, R. *Acta Crystallogr., Sect, B* **1972**, *B28*, 1278. (b) Macchi, P.; Overgaard, J.; Larsen, F. K.; Iversen, B. B. Unpublished results.
(66) Calculations confirm that charges on O are (slightly) less negative in F_2CO_2 compared to H_2CO_2.
(67) A comparative study was recently reported by: Yudanov, Y. V.; Di Valentin, C.; Gisdakis, P.; Rosch, N. *J. Mol. Catal. Sect. A* **2000**, *158*, 189−197.
(68) Abramov, Y. A. *Acta Crystallogr., Sect. A* **1997**, *A53*, 264−272.